MUSCAT EXPERIMENT: ACTIVE FREE FALLING UNITS FOR IN SITU MEASUREMENTS OF TEMPERATURE AND DENSITY IN THE MIDDLE ATMOSPHERE

M. T. Bordogna, L. Fidjeland, M. Fjällid, M. Galrinho, A. Haponen, A. Hou, N. Ivchenko, D. Kristmundsson, Ó. L. Lárusdóttir, M. Lejon, M. Lindh, E. Lozano, P. Magnusson, A. Myleus, B. D. Oakes, and G. Tibert

Royal Institute of Technology (KTH), 100 44 Stockholm, Sweden, muscatexperiment@gmail.com

ABSTRACT

The main scientific objective of the MUSCAT Experiment is to develop a technique to reconstruct temperatures and density profiles in the middle atmosphere using active spherical probes. The MUSCAT experiment was launched on May 9, 2013 on the REXUS-13 sounding rocket from Esrange, in northern Sweden. The experiment ejected four probes that collected raw GPS signal. The experiment design and preliminary results are presented here.

Key words: MUSCAT; GPS; REXUS; KTH.

1. INTRODUCTION

For any study done in the middle atmosphere it is important to have the temperature profile. There are a few ways to obtain middle atmospheric temperatures through methods, each with its advantages and disadvantages. The altitude resolution of satellites and LIDAR measurements is insufficient for regional atmospheric studies. LIDARs are often limited by both clouds and daylight as well as requiring long integration times, up to many hours, to be able to find temperatures; satellites only measure at very sparse vertical locations and they also need complicated retrieval techniques to derive the temperature. There is a strong need for precise in-situ measurements to verify the temperatures derived from remote sensing techniques.

A well known technique for in-situ measurements is based on passive free falling units, usually inflatable spheres with diameter around 1 m with metallized surface to enable the radar to track their position as function of time. However to achieve the accuracy and precision required, the radar must be a high-precision tracking system [2].

The method proposed by MUSCAT is based on active free falling unites using GPS to determine position of the probes with high accuracy. MUSCAT, MUltiple Spheres for Characterization of Atmospheric Temperatures is a sounding rocket experiment developed at the Division of Space and Plasma Physics at the School of Electrical Engineering and the Department of Mechanics at the School of Engineering Sciences at The Royal Institute of Technology (KTH), together with the Department of Meteorology at Stockholm University (MISU).

The primary objectives of the experiment are:

- Proof of concept of a multi-point ejectable subpayload for the derivation of temperature and density profiles in middle atmosphere.
- Observation, using multi-point measurements, of the horizontal structure of temperature and density profiles.

The objective of this paper is to present the MUSCAT Experiment and its preliminary results. In sections 2 and 3 the scientific objectives and experiment timeline are presented. In section 4 the design of the experiment is described. Preliminary results and conclusion are discussed in sections 5 and 6.

2. SCIENTIFIC DESIGN

During the free fall the forces acting on each probe, and the direction of the total velocity vector are illustrated in Figure 1. The forces are the gravity force (mg) and the drag force (F_D) . Using the equation of motion, it is possible to write a system of equations for the forces acting in the vertical and horizontal directions respectively:

$$\begin{cases} ma_V = mg - \frac{1}{2}\rho_\infty A C_D |V_\infty| V_\infty \cos\theta \\ ma_H = \frac{1}{2}\rho_\infty A C_D |V_\infty| V_\infty \sin\theta \end{cases} \quad (1)$$

where m is the mass of the spherical probe, g is the acceleration due to gravity, ρ is the density of the atmosphere, V is the velocity, A is a reference area (maximum cross section area for a sphere) and C_D is the drag coefficient.

The subscript ∞ denotes free-stream conditions. From the vertical component the density can be obtained:

$$\rho_\infty = -\frac{2m(a_V + g)}{AC_D|V_\infty|V_\infty \cos\theta} \quad (2)$$

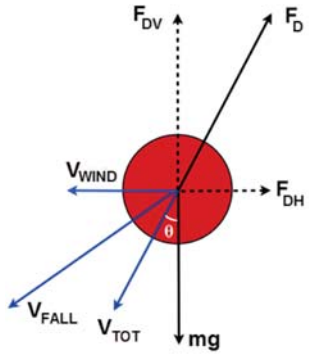

Figure 1. Forces acting on the probe during free fall.

In order to calculate ρ position, velocity and acceleration of the probe must be known. The probes carry internal sensors and an antenna which receives GPS raw signal. Using Eq. (2) one can integrate the hydrostatic equilibrium:

$$\mathrm{d}p = -\rho_\infty g \, \mathrm{d}z \quad (3)$$

where $\mathrm{d}p$ is a differential variation in pressure and $\mathrm{d}z$ is a small change in altitude. Using the equation of state for perfect gas:

$$p = \rho_\infty \frac{R}{M} T_\infty \quad (4)$$

R is the universal gas constant, M is the molar mass and T_∞ is the temperature in the free-stream, one can obtain the temperature profile:

$$T_\infty(h) = T_\infty(0)\frac{\rho_\infty(0)}{\rho_\infty(h)} + \frac{M}{\rho_\infty(h)R}\int_{z(h)}^{z(0)} \rho_\infty g \, \mathrm{d}z \quad (5)$$

where $T_\infty(0)$ and $\rho_\infty(0)$ is the temperature and density at the beginning of the fall, respectively. A detailed derivation of Eq. (5) can be found in appendix of [1].

The coefficient of drag, C_D (Figure 2), has been obtained by gathering accurate experimental data from literature [4], [5] and [6] (estimated error of maximum +/- 2%), for a suitable range of Mach and Reynolds numbers, and by the use of an accurate polynomial for the drag coefficient in creeping flow. Data on the drag coefficient were missing for a small region of low Mach numbers and high Reynolds number (above $2{\cdot}10^6$) which are expected below 10 km altitude. At these high Reynolds numbers the drag coefficient is expected to change very little and the closest value of the drag coefficient for a given Mach number is used.

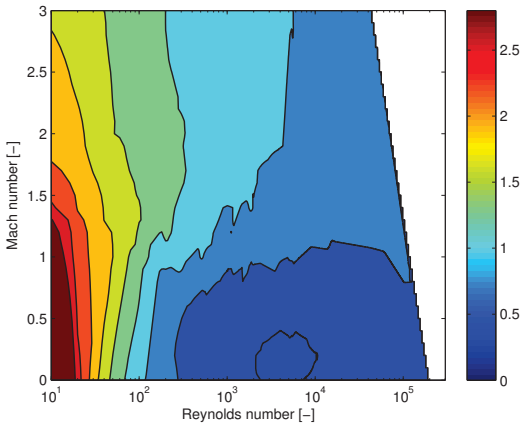

Figure 2. Drag coefficient of the sphere.

3. EXPERIMENT OUTLINE

The experiment involves ejecting four spherical probes, or Free Falling Units (FFUs), from a REXUS rocket module. The module, called Rocket Mounted Unit (RMU), carries the FFUs to an altitude of approximately 60 km where they are ejected from the rocket while it is spinning at 4 Hz. The FFUs will then continue the ascending phase until the apogee at 85 km. The FFUs record raw GPS signal and inertial sensor data as they travel through the atmosphere.

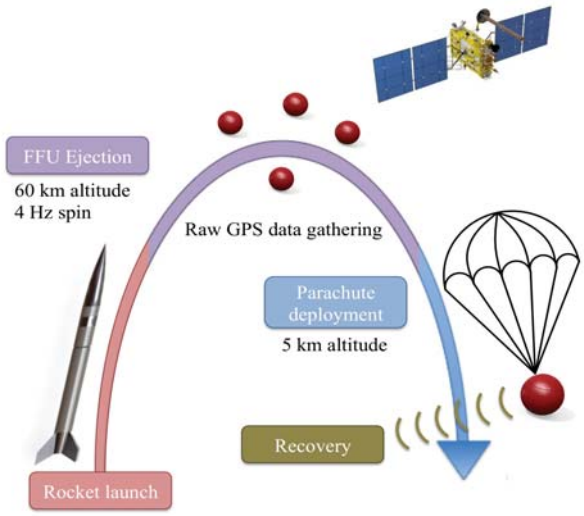

Figure 3. The flight phases of the MUSCAT Experiment.

At an altitude of 5 km the FFUs deploy parachutes and switch from raw GPS data logging to transmitting coordinates from a commercial GPS unit to the recovery team which locates and retrieves them upon landing. The GPS read-out data are then analyzed to obtain velocity and acceleration of the FFUs during the free fall. These data

are used, along with the drag coefficient of the FFUs, to derive the atmospheric density and temperature profiles. The experiment timeline is shown in Figure 3.

4. DESIGN OVERVIEW

The MUSCAT experiment occupies one rocket module in the payload stack. It consists of Rocket Mounted Unit and four Free Falling Units.

4.1. Rocket Mounted Unit (RMU)

4.1.1. Mechanics

The RMU (Figure 4) consists of a rocket cylinder, the ejection system and hatches, a pyrocutter module and rocket mounted electronics.

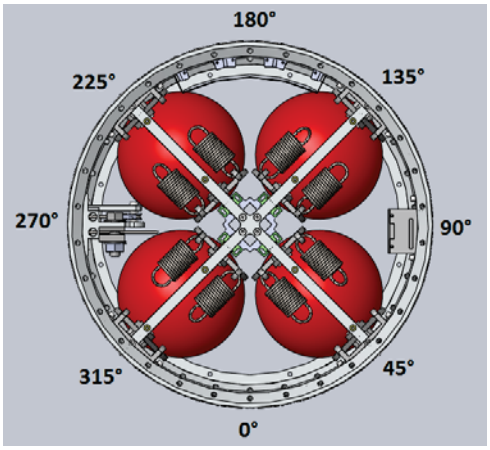

Figure 4. Rocket Mounted Unit (RMU). Openings for the ejection of the FFUs are positioned at 45°, 135°, 225° and 315°. Pycocutter module is positioned at 270° and onboard camera is at 90°.

The rocket cylinder is a REXUS rocket module with 220 mm height and 356 mm diameter, modified to accommodate four openings, a cable groove and additional components (Figure 5). A thorough structural analysis of the strength and stiffness of the rocket module with four 134 mm diameter perpendicular holes on the cylindrical surface shows that increasing the wall thickness from 4 to 8 mm (and locally to 12 mm) ensures the stiffness and strength of the module without reinforcement around the holes. The report of the FEM analysis is presented in appendix of [1].

The ejection system releases the FFUs sideways from the rocket by means of loaded springs. The system consists of a four rails, four collars, 16 extension springs and four FFU cages (Figure 6). Each of the four collars is fixed on the inside of the rocket cylinder, around the openings.

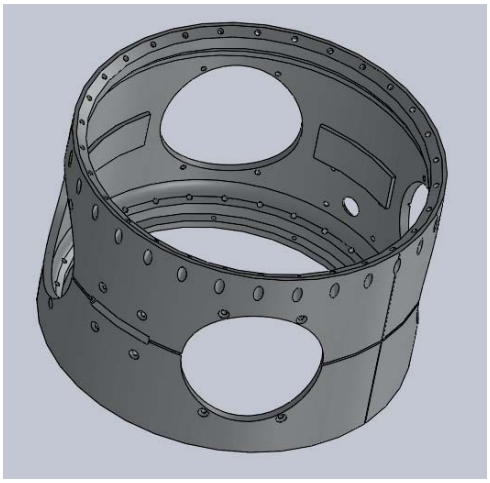

Figure 5. Modified rocket cylinder with four openings, cable groove and additional components.

The rail system consists of two aluminium crosses, with four rails each. The ends of the crosses are fixed to the collar. The FFU cages are constrained by the rails and can slide along them. Extension springs are attached between the inner part of the FFU cages and the collars and pull the FFU out of the rocket during ejection. A hatch is attached to the outer part of the FFU cage and it is ejected with the FFU. The cages are constrained by a 2.5 mm diameter steel cable strapped around the module skin, in the groove and on the hatches.

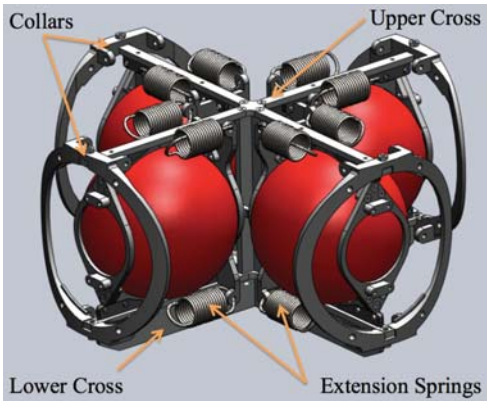

Figure 6. Ejection system with upper and lower crosses, collars and extension springs

This steel cable is cut by two pyrocutters at the ejection time to release the FFUs. To protect other experiments from hot gases and snow, when the hatches have been ejected, two aluminium plates are placed on the upper and the lower part of the rocket module.

The RMU PCB containing the electronics monitoring the FFU is located in the center of the RMU beneath the ejection system. The pin connector is attached to a platform mounted in the middle between the upper and the lower

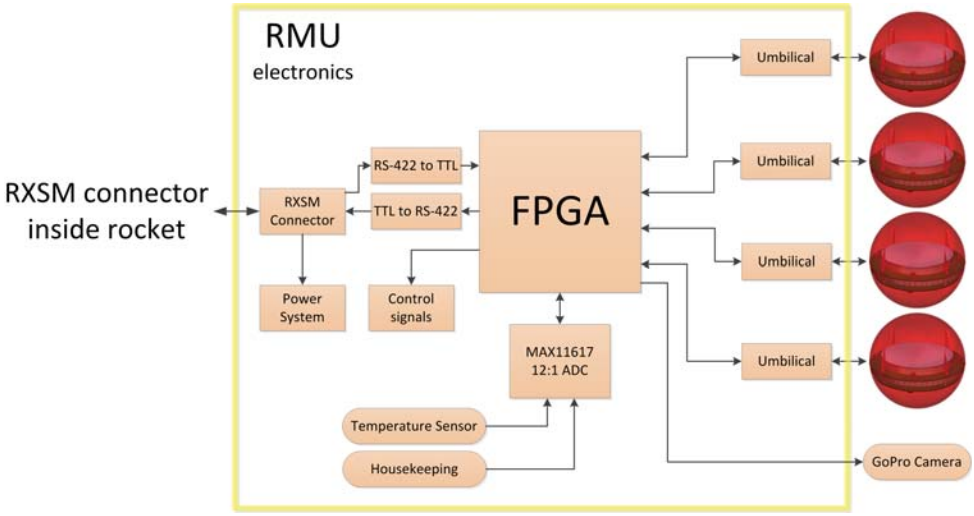

Figure 8. Conceptual diagram of the RMU electronic system.

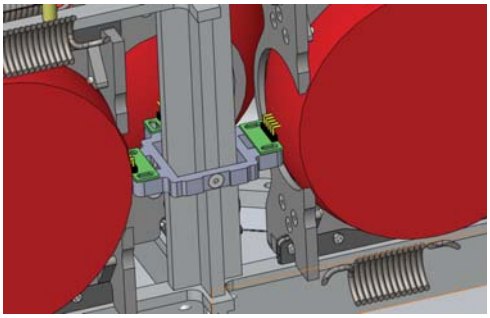

Figure 7. Position of the five pins umbilical connector.

cross of the ejection system and located behind the FFU cage (Figure 7). The receptacle connector is soldered on the top side of the top PCB of the FFU, so it is located along the FFU equator. Since the pin umbilical connectors are fixed, the sliding movement of the FFU cage breaks the connection during the ejection, when the FFUs are ejected.

4.1.2. Electronics

The RMU electronics' most important role is to serve as one part of the interface between the FFUs and ground control station up until ejection. As can be seen in Figure 8, the RMU PCB is connected to the RXSM through a RXSM interface connector and to each FFU. Inside the RMU RS-422 UART signal levels from the RXSM are converted to a standard LVTTL UART to the RMU FPGA. The RMU FPGA works as a data switch which allows commands to be sent from the ground control station and FFUs status to be received at the ground control from one FFU at a time. The FFUs can be charged as needed through the RMU.

The RMU FPGA also controls the RMU housekeeping system and the GoPro HD Hero 3 Black Edition camera that is used to observe the ejection of the FFUs. The RMU housekeeping system monitors the voltages on the RMU PCB and temperatures inside the rocket. This data is sent to the ground control via RXSM and is not saved onboard. The GoPro HD Hero camera is powered by RMU electronics and it is activated via ground control. The footage is stored to the cameras own 64 GB SD card.

4.2. Free Falling Units (FFU)

4.2.1. Mechanics

The FFU is shown in Figure 9. The FFU consists of a spherical structure, a recovery system and a PCB assembly. The FFU is 124 mm in diameter and the mass is 0.44 kg.

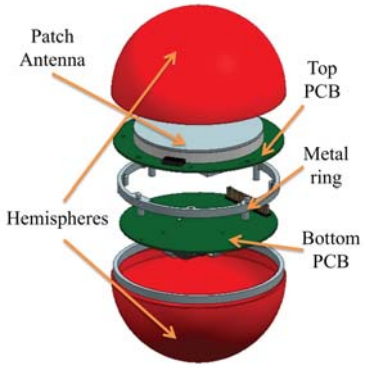

Figure 9. Free Falling Uunit explosion view with hemispheres, top PCB, bottom PCB, metal ring and patch antenna.

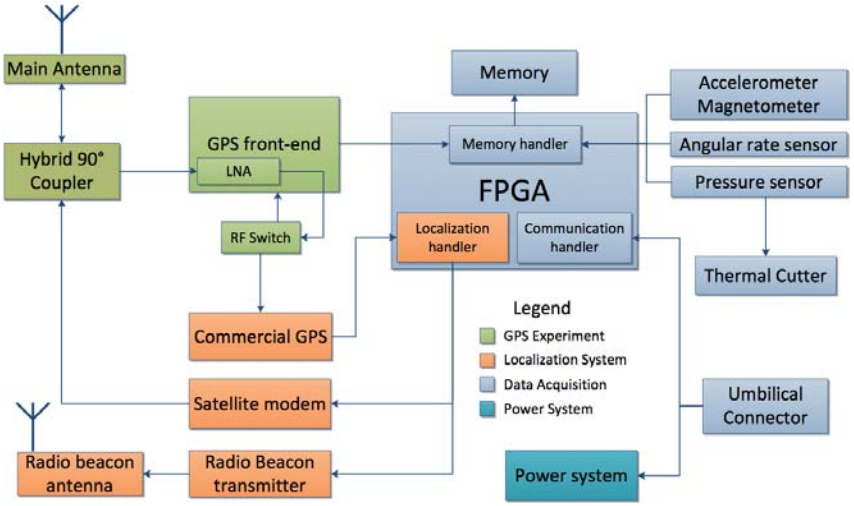

Figure 10. Schematic diagram of FFU system.

The FFU electronics is distributed between the top PCB (D=121 mm), and the bottom PCB (D=112 mm), interconnected by a vertical header/receptacle connector. The antenna is placed on the upper surface of the top PCB and the battery is mounted beneath the bottom PCB using a cage. The two PCBs are screwed onto a metal ring (Figure 11).

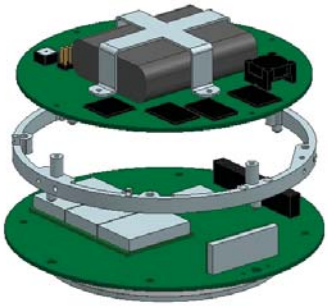

Figure 11. PCB assembly with all large electrical components, upside-down.

The two hemispherical shells that create the outer shape of the FFU are made of Glass Fiber Reinforced Polymer (GFRP). The shells are manufactured in house by Vaccum Assisted Resin Transfer Molding to achieve a controlled outer surface. Three ply symmetrical layup results in a shell thickness of 1.2 mm. High temperature resistant epoxy (Tg up to 220° C) is used.

During flight, the parachute is housed inside the upper hemisphere of the FFU. For the assembly of the upper hemisphere with the PCB assembly a fishing line (Spectra Fiber Rope) has to pass through the holes marked 1-10 as shown in Figure 12. The line is tightened using a custom made winch. On its path the fishing line goes also through a custom made thermal cutter placed under the

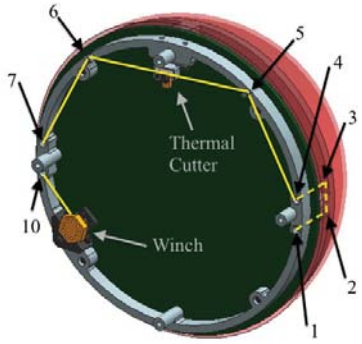

Figure 12. Nylon string securing the upper hemisphere to the PCB assembly.

top PCB. Once the FFU reaches the parachute deployment altitude the thermal cutter is activated. When the vertical constraint on the upper hemisphere is removed the parachute is deployed. A single Top Flight ThinMill 30 X-shape is used for each FFU. A cross parachute has been selected based on its low drift.

4.2.2. Electronics

All the FFUs have the same electronic system. In each FFU there is a GPS experiment, localisation, data acquisition and power system, see Figure 10. The primary objective of the electrical system is to receive and store raw GPS data. This is done with the GPS experiment system which is positioned on the top PCB and consists of a main antenna, GPS front end and a RF switch.

Figure 13. Panorama picture of the ejection of the four FFUs.

The main antenna is a custom made patch antenna with hybrid 90 degree coupler, two feeds and a substrate with ϵ_r=1 is used. These characteristics allow the antenna to transmit LHCP (left hand circular polarization) at 1615 MHz, Globalstar frequency, and receive RHCP (right hand circular polarization) at 1575.42 MHz, L1 GPS frequency. The main antenna is less directive than most patch antennas.

The raw GPS signal received at the main antenna is filtered, mixed and digitized in the GPS front end receiver MAX2769 from Maxim. First the signal is amplified in a low noise amplifier. Then it is routed out of the front-end and through a RF switch of type PE4230 from Peregrine. The switch is controlled from the FPGA and makes it possible to choose if the signal is routed back into the front-end or to a commercial GPS receiver which is used by the localisation system. When the signal is sent back to the front end it is mixed down to a desirable intermediate frequency. The outcome is then sampled and digitized and sent into the FPGA to be written to the memory.

The data acquisition system is positioned on the bottom PCB and monitors all voltages and currents and saves it to memory. Furthermore it contains angular rate sensors, accelerometer with inbuilt magnetometer and a pressure sensor. The data from these sensors are stored to memory. The pressure sensor is used to trigger the thermal cutter when the pressure has risen to a certain value. The thermal cutter is a metal wire which melts the fishing line thus releasing the parachute.

The localisation system is positioned on the top PCB and is activated after parachute deployment. The RF signal from the main antenna is then routed to the commercial GPS receiver of type ET-318 from GlobalSat. This all in one GPS receiver can after fast setup acquire the position of the FFU and send it to the FPGA. The position is then sent through an STX2 satellite modem from Axonn via the main antenna at 1615 MHz. The STX2 can send short messages of up to 9 bytes to the Globalstar service. The satellite messages containing the FFUs positions are routed to a FTP server and displayed on a webpage using Google maps. This provides an easy to follow tracking of the FFUs. For redundancy a radio beacon transmitter of type TX1 from Radiometrix also transmits the acquired position modulated into its VHF signal at 173.250MHz, 173.275MHz, 173.300MHz and 173.325MHz, one frequency for each FFU. The TX1 transmitter chip is used with a radio beacon antenna which is a one fourth the wavelength long monopole. This makes it possible to take a bearing on a FFU when using a directed receiver antenna at the same frequency. The power system makes sure the FFUs battery will last throughout the mission and sees to that all systems are kept at correct voltage levels.

5. RESULTS

5.1. Ejection of the FFUs

Ejection of the FFUs occurred at t+67s when the REXUS 13 was at 58 km altitude and the ejection mechanism performed nominally (Figure 13). All FFUs were ejected and hatches separated from the FFUs after the ejection. Upon ejection all FFUs were subjected to air drag, this can be seen in Figure 14, where in the first seconds after ejection the acceleration is negative. In Figure 14 it can also be seen that the FFUs have the antennas facing up since the acceleration is positive during reentry.

At ejection the rocket was spinning at 3.2 Hz, however the spin rate of the FFUs around the z-axis is lower, between 2.3 and 1.8 Hz, depending on FFU. During the reentry phase the spin rate decreased, this is due to the fact that the increasing air density leads to higher air drag acting on the FFUs. On the x and y axis it is possible to see a clear precession motion of the FFU. In Figure 15 it is possible to see that all FFUs have a negative value of angular rate around the y-axis at ejection. This means that the ejection system introduced a small torque during the ejection. However this did not disturb the dynamic of the free fall.

5.2. Landing and recovery

Parachute deployment performed nominally for all FFUs. Upon deployment all FFUs switched from GPS experiment to commercial GPS. The positions of the FFUs after parachute deployment can be seen in Figure 16. The total descent last between 16 and 21 minutes and the FFUs drifted between 10.2 and 26.2 km..

Signal from the beacon transmitter was lost approximatively two minutes before the actual landing of the FFUs,

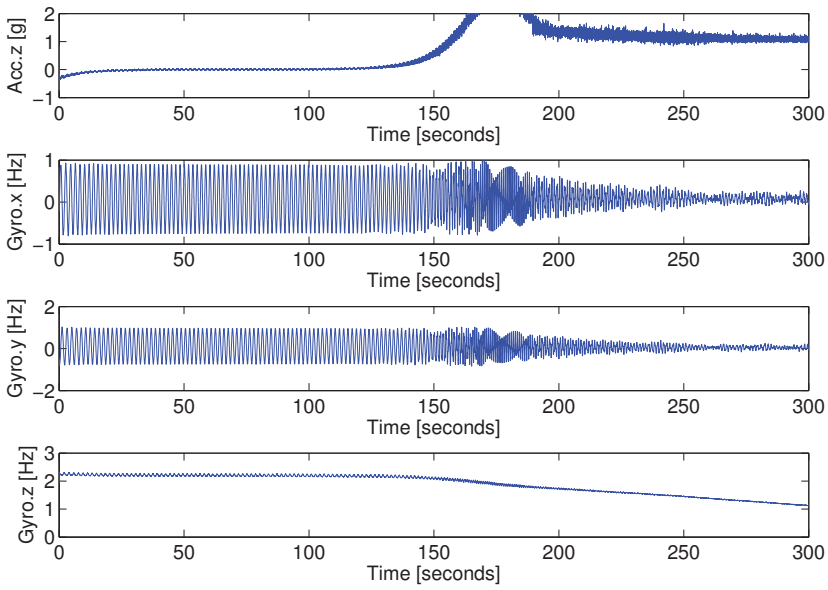

Figure 14. Inertial sensor data of a flight FFU: acceleration in z direction and x, y and z component of the angular rate.

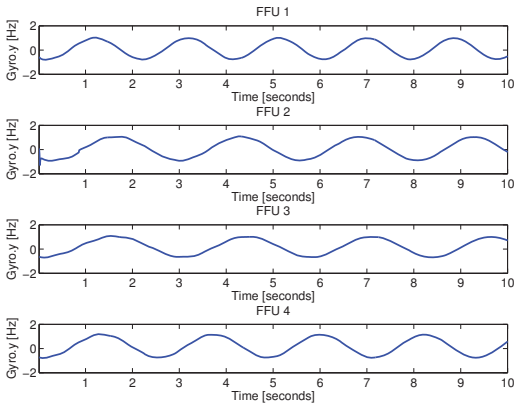

Figure 15. Angular rate around y-axis for the first 10 seconds after ejection.

however modem satellite messages were received until landing. The beacon transmitter signal was lost at low altitudes due to trees and hills between the FFUs and the antenna receiver at Esrange. In those two minute the FFUs drifted between 1 and 4 km depending on FFU.

5.3. GPS experiment

The four FFUs collected raw GPS data from 5 to 9 satellites during the free fall. The data from two of those satellites are shown in Figure 17. The post processed signal is more or less constant for these two satellites except for the high frequency oscillations. These oscillations have the same period as the precession motion of the FFU.

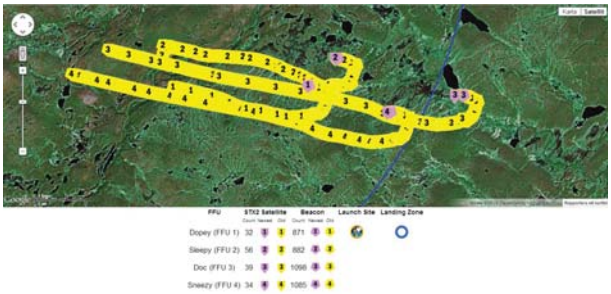

Figure 16. Positions of the four FFU from parachute deployment to landing.

For some other satellites the post-processed signal is not constant, which implies a loss of tracking. In most cases this can be solved with better post processing. In the initial analysis the position and velocity of the FFU have only be found for a limited time interval. One of these interval is shown in Figure 18. In Figure 18 is shown also the simulation of free fall obtained using the C_D introduced in section 2 and the standard atmosphere model.

The discrepancy in the altitude and velocity between the experiment and simulation is believed to mainly be caused by a difference in density between the standard atmosphere and the atmosphere above Kiruna the day of

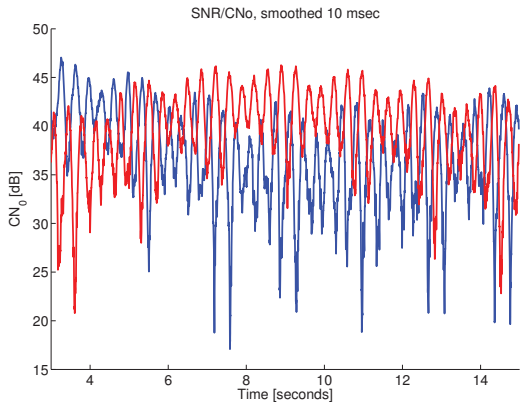

Figure 17. Post-processed signal to noise ratio for two satellites.

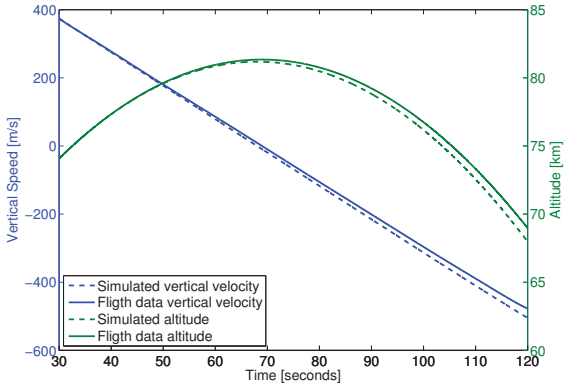

Figure 18. Altitude and vertical velocity of the FFU during free fall from flight data and simulation.

the launch. Additional sources of error can be effects due to wind, the 2% error induced by the estimated value of the drag coefficient or a small difference in the gravitational constant used in the simulation compared to the one at Kiruna. The temperature in the atmosphere may also be different than the standard atmosphere, giving a slightly different Mach number and in turn a slightly different drag coefficient. The temperature and density profiles will be obtained in future post-processing of the experimental results.

6. CONCLUSION

The experiment has proven its functionality and all systems and subsystems performed nominally. One of the four FFU malfunctioned during the flight and part of the flight data are missing. However this did not compromise the experiment data from three FFUs are sufficient to obtain the horizontal structure of temperature and density.

Raw GPS data have been saved in the Free Falling Units and preliminary results shown that the data can be used to derive position, velocity and acceleration of the falling probes. Future work includes the complete evaluation of position, velocity and acceleration for all the probes. These data will be used in the derivation of temperature and density profiles as described in section 2. Moreover GPS results will be used to capture horizontal wind data at different altitudes.

ACKNOWLEDGMENTS

The MUSCAT team has two special thanks. First we would like to thank all the personnel of the Division of Space and Plasma Physics, the Mechanics Department and the Division of Lightweight Structures for the support and the access to the laboratories. Second we would like to thank the sponsors of the REXUS/BEXUS program, SNSB, DLR, SSC and ESA, that allowed us to start this incredible adventure. Thanks also the the external sponsors that provided the MUSCAT Team with materials and components.

REFERENCES

[1] Ó.L.Lárusdóttir et al., *MUSCAT Student Experiment Description*, Royal Institute of Technology (KTH), 4.1 ed., April 2013.

[2] Schmidlin F. J., et al., 1991, *The Inflatable Sphere: A Technique for the Accurate Measurement of Middle AtmosphereTemperatures*, Journal of geophysical research, vol. 96, Dec.1991.

[3] F. L. Bartman. et. al., *Upper-Air Density and Temperature by the Falling-Sphere Method*, Journal of Applied Physics, vol. 27, no. 7, 1956.

[4] A.B. Bailey and J. Hiatt. *Free-flight measurements of sphere drag at subsonic, transonic, supersonic and hypersonic speeds for continuum, transition and near-free-molecular flow conditions*, Technical report, Von Karman Gas dynamics facility, 1971.

[5] W. R. Lawrence. *Free-flight range measurements of sphere drag at low Reynolds numbers and low Mach numbers*, Technical report, Von Karman Gas dynamics facility, 1967.

[6] K. L. Goin and W. R. Lawrence. *Subsonic drag of spheres at reynolds numbers from 200 to 10,000*, AIAA Journal, 6(5):961962, 1968.